Inorganic Chemistry

ARTICLE

pubs.acs.org/IC

Sulfonated Diiron Complexes as Water-Soluble Models of the [Fe−Fe]-Hydrogenase Enzyme Active Site

Michael L. Singleton, Danielle J. Crouthers, Robert P. Duttweiler, III, Joseph H. Reibenspies, and Marcetta Y. Darensbourg*

Department of Chemistry, Texas A&M University, College Station, Texas 77843, United States

Supporting Information

ABSTRACT: A series of diiron complexes developed as fundamental models of the two-iron subsite in the [FeFe]-hydrogenase enzyme active site show water-solubility by virtue of a sulfonate group incorporated into the $-SCH_2NRCH_2S-$ dithiolate unit that bridges two $Fe^I(CO)_2L$ moieties. The sulfanilic acid group imparts even greater water solubility in the presence of β-cyclodextrin, β-CyD, for which NMR studies suggest aryl-sulfonate inclusion into the cyclodextrin cavity as earlier demonstrated in the X-ray crystal structure of **1Na**·2 β-CyD clathrate, where **1Na** = $Na^+(\mu\text{-}SCH_2N(C_6H_4SO_3^-)CH_2S\text{-})[Fe(CO)_3]_2$, (Singleton et al., *J. Am. Chem. Soc.* **2010**, *132*, 8870). Electrochemical analysis of the complexes for potential as electrocatalysts for proton reduction to H_2 finds the presence of β-CyD to diminish response, possibly reflecting inhibition of structural rearrangements required of the diiron unit for a facile catalytic cycle. Advantages of the aryl sulfonate approach include entry into a variety of water-soluble derivatives from the well-known $(\mu\text{-SRS})[Fe(CO)_3]_2$ parent biomimetic, that are stable in O_2-free aqueous solutions.

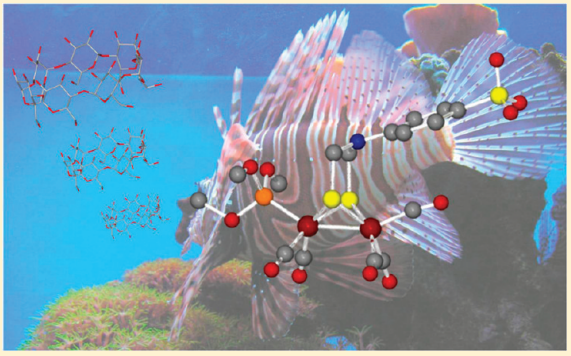

INTRODUCTION

The synthesis of new small molecule models of the diiron hydrogenase enzyme active site[1] is driven by a desire to better understand a unique biological system capable of producing hydrogen at rates comparable to platinum.[2] In doing so the ultimate goal is the development of iron- and sulfur-based molecular catalysts for use in the cathode of solar powered water electrolysis cells.[3] To date hundreds of these small molecule models of the form $(\mu\text{-}SCH_2XCH_2S)[Fe(CO)_{3-n}L_n]_2$ (X = CR_2, NR, O, or S) have been synthesized and their proton reduction capabilities analyzed through a combination of electrochemical and spectroscopic techniques.[4,5] While it might seem reasonable to conduct these assays in water to match the ideal environment of the hydrolysis cells, the proton reduction experiments conducted on the diiron model systems have been limited almost entirely to organic solvents or mixtures of water and MeCN. This limitation is due to the inherent insolubility of the majority of small molecule models in water, which results from their hydrophobic nature, as well as inherent complexities with water as solvent in electrochemical studies. In fact, over the past 10 years only a handful of water-soluble complexes have been described.

The dianionic complex $(\mu\text{-pdt})[Fe(CO)_2CN]_2^{2-}$, ($\mu$-pdt = $-S(CH_2)_3S-$) synthesized from CO substitution in $(\mu\text{-pdt})[Fe(CO)_3]_2$ (**1**) by CN^-, was described as highly water-soluble by Pickett and co-workers in 1999.[6] In the interim there have been no further reports of work exploring the aqueous, proton reduction catalysis capability of the cyanide-containing diiron complexes, likely because of the sensitivity of these compounds to both air and acid. There have, however, been several approaches toward developing more hydrophilic complexes that exhibit greater stability than the cyanide derivatives.

Phosphine ligands have long been used in the $[Fe-Fe]\text{-}H_2$ase model systems as a synthetic substitute for the naturally occurring CN^- ligands.[1] The degree of substitution has been shown to play an important role in fine-tuning the proton reduction capabilities of hundreds of models of the enzyme active site. Disubstituted $(\mu\text{-pdt})[Fe(CO)_2L]_2$ complexes typically reduce protons from HOAc at the initial Fe^IFe^I/Fe^IFe^0 reduction, but with a large overpotential.[7] Monosubstituted complexes on the other hand can still reduce protons at the first reduction event but at a lower overpotential than disubstituted complexes.[8] Specialized ligands such as phosphatriazaadamantane (PTA), tris(hydroxymethyl)phosphine, and $Ph_2P(C_6H_4SO_3^-)$ have been shown to increase water solubility in a variety of metal complexes.[8−10] In the case of PTA, the ligand alone did not impart significant solubility to $(\mu\text{-pdt})[Fe(CO)_3]$ $[Fe(CO)_2TA]$ in pure water; however, it did permit studies in mixtures of $MeCN/H_2O$ of up to a 1:3 ratio where the proton reduction capabilities of the complexes were observed to shift to significantly more positive potentials with increasing amounts of water.[8] Sun and co-workers

Received: February 8, 2011
Published: April 27, 2011

 © 2011 American Chemical Society

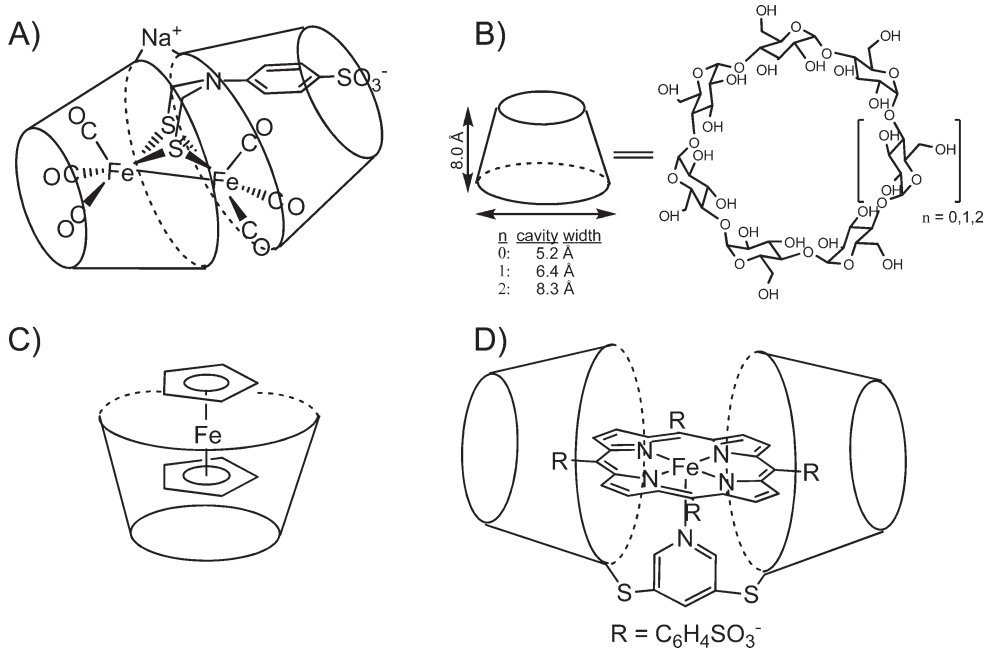

Figure 1. (A) Cartoon of X-ray crystal structure of sulfonated diiron hexacarbonyl complex, **1A**, encapsulated within two β-cyclodextrins.[12] (B) Diagram of α-, β-, and γ-cyclodextrins.[13] (C) Structure of ferrocene in β-cyclodextrin.[14] (D) Cartoon of the O_2-binding iron-porphyrin biomimetic cyclodextrin system developed by Kano and co-workers. R = -*p*-$C_6H_4SO_3^-$.[16]

further used the di-N-acetylated phosphatriazaadamantane (DAPTA) ligand to impart moderate solubility of $((\mu\text{-pdt})[\text{Fe}(\text{CO})_2\text{L}]_2$ in water which allowed the first electrochemical studies in 100% water (0.05 M *n*-Bu_4NPF_6 solution).[9] These studies indicated that water played a significant role in altering both the reduction potential and the electrocatalytic response of the model complexes, with the reduction of protons occurring more positive than the initial Fe^IFe^I/Fe^IFe^0 reduction as a result of the protonation of the amines in the PTA and DAPTA ligands.

While successful for developing less hydrophobic diiron model systems, the ligand-based solubilization technique limits the variety of complexes that might be synthesized. In contrast, incorporation of a water-solubilizing group into the dithiolate linker appears to offer more versatility. By modifying D-glucopyranoside to include a dithiolate unit Weigand and co-workers were able to obtain sugar functionalized diiron models.[11] These species, initially synthesized as the protected tetra-O-acetyl derivatives, showed greatly increased hydrophilicity upon deprotection of the hydroxyl units. Unfortunately, the deprotected species was not stable in protic solvents, thus limiting its applicability.

Recently, we described the synthesis of a diiron model complex containing an aryl sulfonate modified azadithiolate linker, $Na^+(\mu\text{-SCH}_2\text{N}(\text{C}_6\text{H}_4\text{SO}_3^-)\text{CH}_2\text{S-})[\text{Fe}(\text{CO})_3]_2$, **1Na**.[12] While the addition of this moiety into the parent hexacarbonyl complex renders it insoluble in most nonpolar organic solvents, it imparts moderate solubility (~1.1 mM) in pure water. Additionally, the complex remains stable for an extended period of time in deaereated water (up to several months when stored in the refrigerator), allowing study of the diiron complex in water by NMR, IR, UV−vis, and electrochemical methods. Additionally, the aryl sulfonate group promoted inclusion of the complex in β-cyclodextin leading to the structural characterization of a **1Na**·2 β-cyclodextrin clathrate, which showed the aryl sulfonate group penetrating through the cavity of one of the cyclodextrins, Figure 1A. As expected, the interaction with the cyclodextrin greatly increased the water solubility of **1Na** and opened the possibility for using the inclusion in the cavity to mimic the protein environment of the enzyme.

Cyclodextrins, cyclic oligosacharides consisting most commonly of 6−8 glucose units, have properties long recognized as ideal for biomimetics, Figure 1B.[13] Their hydrophobic cavities, ranging in diameter from 4.5 to 9.5 Å, depending on the number of glucose units, and having a height of ~8.0 Å, have in fact been demonstrated to serve as hosts for organometallics.[14] The hydrophilic hydroxyl rims provide hydrogen bonding sites.[15] An important example is the inclusion of ferrocene in α-, β-, and γ- cyclodextrins, the adducts of which have all been structurally characterized, Figure 1C . In all three adducts, the cyclodextrins incorporated at least one of the cyclopentadienyl rings of ferrocene, affecting the spectroscopic and electrochemical properties of the organometallic unit.

Furthermore inclusion in the cyclodextrins can provide similar site isolation as active site cavities in proteins. A recent example of this application, the one that was inspirational for our work, was reported by Kano and co-workers, Figure 1D.[16] Through the inclusion of an iron tetrakis(4-sulfonatophenyl)porphyrin inside a dimeric cyclodextrin system, where the two cyclodextrins were connected at the 2 position via a pyridine linker, they showed that the cyclodextrin super structure provided a high degree of site isolation and allowed the iron porphyrin to bind oxygen in water without forming the commonly observed μ-oxo dimers. While the intriguing cyclodextrin-containing biomimetic models such as this are not common, the inherent inclusion properties of cyclodextrins and the extensive literature on methods to modify them make them attractive targets for exploring the effects of inclusion in a cavity on models of [Fe−Fe]-hydrogenase.

In the present work we have used the sulfonated hexacarbonyl complex, **1Na**, as a precursor to generate a series of phosphine-substituted complexes of the type $Na(\mu\text{-SCH}_2\text{N}(\text{C}_6\text{H}_4\text{SO}_3)\text{-CH}_2\text{S-})[\text{Fe}(\text{CO})_3][\text{Fe}(\text{CO})_2\text{L}]$ (L = $P(OMe)_3$ (**2Na**); PTA

dx.doi.org/10.1021/ic200272x |*Inorg. Chem.* 2011, 50, 5015–5026

(**3Na**); and PPh_3 (**4Na**) and $Na(\mu\text{-}SCH_2N(C_6H_4SO_3)CH_2\text{-}S\text{-})[Fe(CO)_2PMe_3]_2$ (**5Na**), that have varying degrees of water solubility. Through structural analysis and electrochemical studies in MeCN we show that the sulfonate group can impart modest water solubility to complexes **2Na**, **3Na**, and **5Na** without drastically altering their structural or electrochemical properties. The addition of the large hydrophobic PPh_3 ligand, however, overwhelms the effects of the sulfonate group and renders the model complex insoluble in H_2O.

Additionally, to expand on our previous study,[12] the interaction of the complexes with cyclodextrins is studied in H_2O through NMR spectroscopy and cyclic voltammetry, to determine the effect of cyclodextrin on the phosphine-substituted complexes. All of the complexes show distinct changes in their proton resonances, with **2Na** and **3Na** behaving similarly to **1Na**. The **5Na** complex on the other hand shows different changes, and the specific interaction with cyclodextrin is not as well-defined. For complex **4Na**, the aqueous solubility is only slightly improved in the presence of cyclodextrin, limiting the study of the interaction by NMR.

For the electrochemical studies, our initial hypothesis was that, because of the generally weaker Fe—Fe bond in substituted complexes and the possibility of hydrogen bonding interactions in the $P(OMe)_3$ and PTA derivatives, the cyclodextrins might induce changes in the electrochemical properties of the model complexes by influencing the variety of conformations proposed to occur in the electrocatalytic cycle.[17] As will be shown, it appears that the effect of the cyclodextrin is to hinder proton reduction rather than facilitate it, likely by (a) preventing the structural rearrangements needed in the catalytic cycle; (b) by inhibiting proton delivery processes within the cavity; or (c) both.

EXPERIMENTAL SECTION

General Experimental Procedures. All solvents used were purified and degassed via a Bruker solvent system. Unless otherwise stated, all syntheses and manipulations were performed using standard Schlenk-line and syringe/rubber septa techniques under N_2 or in an argon atmosphere glovebox. Complexes **1Na** and **1TEA** were synthesized according to recently published procedures.[12] β-cyclodextrin was purchased from TCI America and used without further purification. All other reagents were purchased from Aldrich Chemical Co. and used as received. High resolution electrospray ionization mass spectrometry (HRMS) analysis was performed by the Laboratory for Biological Mass Spectrometry at Texas A&M University. Infrared spectra were recorded on a Bruker Tensor 37 spectrometer in either CaF_2 or NaCl solution cells with a 0.1 mm path length. ^1H NMR spectra were acquired on an Inova 500 spectrometer operating at 500 MHz. All NMR samples were prepared in either D_2O or DMSO. ^1H chemical shifts are reported in parts per million relative to H_2O (4.79 ppm) or DMSO (2.50 ppm).

Voltammograms were obtained using a standard three electrode cell under argon at room temperature using a Bioanalytical System (BAS) 100 electrochemical workstation with a glassy carbon working electrode and a platinum wire auxiliary electrode. For aqueous work, a saturated KCl Ag/AgCl reference electrode was used, and the supporting electrolyte solution was 0.01 M NaCl. Samples were run at a concentration of ~0.1 mM because of their low solubility in the NaCl buffer solution. Between each scan the glassy carbon electrode was removed and polished using a 1 μm polycrystalline diamond suspension and rinsed with both acetone and deionized water to remove any adsorbed material. All aqueous potentials are reported relative to the Ag/AgCl couple as 0.00 V. For work done in MeCN, a saturated $Ag/AgNO_3$ reference electrode was used and the supporting electrolyte solution was 0.1 M Et_4NBF_4. All samples in MeCN were run at a concentration of 2 mM, and potentials are reported relative to the Fc/Fc^+ couple as 0.00 V.

Water solubility studies of the diiron complexes were performed using a Shimadzu UV-2450 UV—vis spectrometer. Deaerated water was added to known amounts of each complex until no solid material was visible in solution. This stock solution was then used to generate several samples of known concentrations allowing the molar absorptivities for each absorption band in the UV—vis spectra to be calculated. Maximum concentrations were obtained by adding enough of each complex to 20 mL of deaerated water that solid remained even after sonicating each sample for 10 min. The slurry was then centrifuged for 30 min or until no suspended solid was visible in solution. The UV—vis spectrum of the supernatant was recorded, and Beer's law was used to calculate the concentration.

X-ray Diffraction Studies. For complexes **2TEA** and **5TEA** low-temperature (110 K) X-ray data were obtained on a Bruker Apex-II CCD based diffractometer (Texas A&M University) (Mo sealed X-ray tube, Kα = 0.71073 Å). For complexes **1Na**, **3TEA**, and **4 TEA** low-temperature (110 K) X-ray data were obtained on a Bruker-D8 Adv GADDS general-purpose three-circle X-ray diffractometer (Texas A&M University) (Cu sealed X-ray tube, Kα = 1.54184 Å). Space groups were determined on the basis of systematic absences and intensity statistics, and structures were solved by direct methods and refined by full-matrix least-squares on F^2. All non-hydrogen atoms were refined with anisotropic thermal parameters. H atoms were placed at idealized positions and refined with fixed isotropic displacement parameters; anisotropic displacement parameters were employed for all non-hydrogen atoms. Complexes **1Na** and **2TEA** were found as racemic twins (BASF = 0.23126 and 0.45113, respectively). Solvent molecules in **2TEA** and **5TEA** presented with significant disordering and were SQUEEZEd out using Platon.[18] The following programs were used: data collection, APEX2[19a] and GADDS,[19b] data reduction, SAINT[19c]; absorption correction and twin refinement, SADABS[19d] and TWINABS;[19d] cell refinement SHELXTL;[19d] structure solutions, SHELXS-97[19d] (Sheldrick); and structure refinement, SHELXL-97[19d] (Sheldrick). The final data presentation and structure plots were generated in X-Seed Version 1.5.[20]

SYNTHESES

Crystallization of $Na(\mu\text{-}SCH_2N(C_6H_4SO_3)CH_2S\text{-})[Fe(CO)_3]_2$ (1Na). **1Na** was synthesized according to the recently described procedure.[12] Wet **1Na** was dissolved to saturation in THF. Crystals of X-ray quality were obtained by cooling this solution at 5 °C overnight.

Synthesis of $Na(\mu\text{-}SCH_2N(C_6H_4SO_3)CH_2S\text{-})[Fe(CO)_3][Fe(CO)_2P(OMe)_3]$, (2Na). To a 100 mL Schlenk flask containing **1Na** (0.250 g, 0.443 mmol) and trimethylamine-*N*-oxide (0.050 g, 0.066 mmol) was added MeCN (20 mL) resulting in a dark red solution. After stirring for 10 m at 22 °C, $P(OMe)_3$ (0.10 mL 0.090 mmol) was added. IR analysis of the solution showed bands as follows: ν(CO) in MeCN: 2050 m, 1994 s, 1973 sh, 1940 w. The reaction was stirred for 30 m after which time the solvent was removed in vacuo. The resulting solid was completely dissolved in tetrahydrofuran (THF) and loaded onto the top of a silica column (4 cm ×20 cm). The dark red product was eluted with MeOH, and solvent was removed with a rotary evaporator to yield 0.115 g (0.174 mmol, 39.2%) of the pure product. The Et_4N^+ salt (**2TEA**) was prepared in an analogous manner starting from **1TEA**. Crystals of X-ray quality were obtained by slow diffusion of ether into a CH_2Cl_2 solution of **2TEA**. IR (THF) ν(CO): 2048 (m); 1992 (s); 1971 (m); 1942 (w), cm^{-1}; ^1H NMR (DMSO): 3.72 (d, J_{HP} = 11.2, 9H);

dx.doi.org/10.1021/ic200272x |*Inorg. Chem.* 2011, 50, 5015–5026

Scheme 1. Synthesis of Phosphine Substituted Complexes 2Na−5Na: (A) (1) Me_3NO, MeCN (2) $P(OMe)_3$; (B) PTA, MeOH, Δ; (C) (1) Me_3NO, MeCN (2) PPh_3; (D) PMe_3, THF, Δ

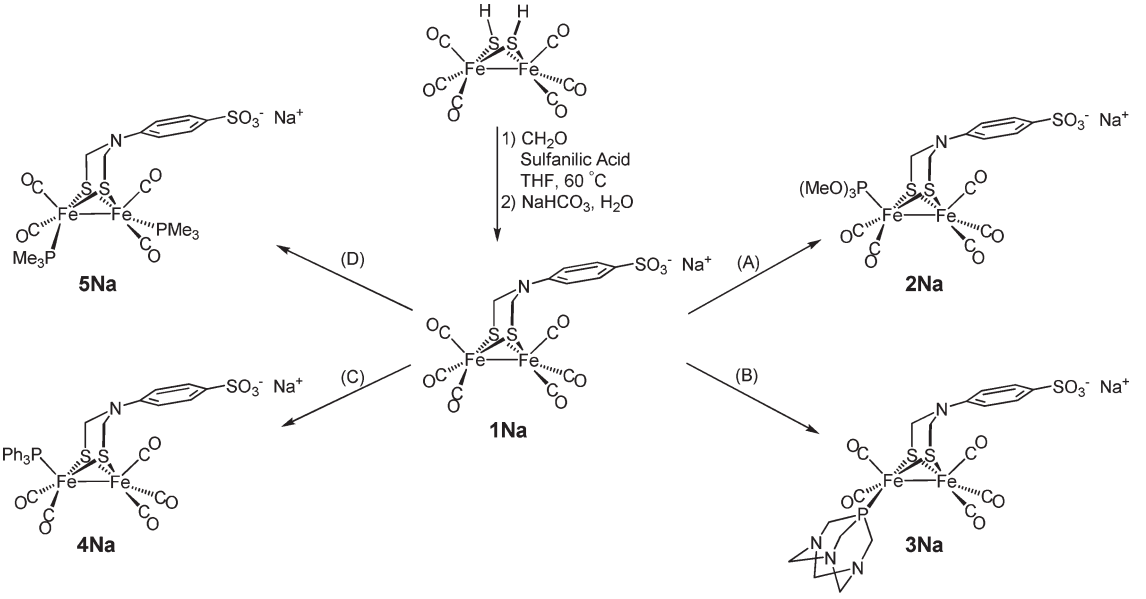

4.35 (d, J = 10.8 Hz, 2H); 4.38 (d, J = 10.8 Hz, 2H) ppm; 6.79 (d, J = 8.3 Hz, 2H); 7.46 (d, J = 8.3, 2H); Electronic absorption spectrum (H_2O): λ_{max} (ε, M^{-1} cm^{-1}) 483 (1450), 335 (8230), 308 (11800), 274 (13310), HRMS (ESI) m/z calcd for $C_{16}H_{17}Fe_2NO_{11}PS_3^{1-}$ Theoretical Mass: 637.8400 g/mol; Found Mass: 637.8371 g/mol.

Synthesis of Na(μ-$SCH_2N(C_6H_4SO_3)CH_2S$-)[$Fe(CO)_3$][$Fe(CO)_2$-PTA], (3Na). To a slurry of **1Na**, (0.200 g 0.355 mmol) in MeOH (20 mL) was added PTA, (0.111 g, 0.704 mmol). The solution was then heated to 60 °C, and the reaction was monitored by IR spectroscopy. The reaction mixture was stirred overnight (~20 h) after which time IR analysis of the solution indicated that it contained primarily the monosubstituted diiron complex as well as a small amount of the starting material. The solvent was removed in vacuo, and the residue was dissolved in THF and loaded onto the top of a silica column (4 cm ×20 cm). Elution with methanol gave two bands which contained, in order, the unreacted starting material and then the product **3Na**. The fractions containing the second band were concentrated to ~3−5 mL on a rotary evaporator and ether was added resulting in a red precipitate. The solid was dried under vacuum to yield 0.108 g (0.156 mmol, 43.8%) of **3Na**. The Et_4N^+ salt (**3TEA**) was synthesized by counterion exchange using Et_4NCl in CH_2Cl_2. Crystals of X-ray quality were obtained by slow diffusion of ether into a concentrated CH_2Cl_2 solution of **3TEA**. IR (THF) ν(CO): 2042 (m); 1986 (s); 1967 (sh); 1930 (w) cm^{-1}; ^1H NMR (DMSO): 4.05 (s, 6H); 4.21 (d, J = 13.2 Hz, 2H); 4.38 (d, J = 12.7 Hz, 3H); 4.46 (d, J = 12.7 Hz, 3H); 4.51 (d, J = 13.2 Hz, 2H); 6.76 (d, J = 8.8 Hz, 2H); 7.44 (d, J = 8.8 Hz, 2H) ppm; Electronic absorption spectrum (H_2O): λ_{max} (ε, M^{-1} cm^{-1}) 500 (540), 346 (2880), 275 (5560); HRMS (ESI) m/z calcd for $C_{19}H_{20}Fe_2N_4O_8PS_3^{1-}$ Theoretical Mass: 670.8880 g/mol; Found Mass: 670.8847 g/mol.

Synthesis of Na(μ-$SCH_2N(C_6H_4SO_3)CH_2S$-)[$Fe(CO)_3$][$Fe(CO)_2$-PPh_3], (4Na). To a 100 mL Schlenk flask containing **1Na** (0.100 g, 0.177 mmol), trimethylamine-*N*-oxide (0.015 g, 0.200 mmol), and PPh_3 (0.051 g, 0.195 mmol) was added MeCN (20 mL), and the solution was heated to 60 °C. IR analysis of the solution showed bands as follows: ν(CO) in MeCN: 2048 m, 1990 sh, 1931 w. The reaction was allowed to stir for 30 min, after which time the solvent was removed in vacuo. The resulting red solid was completely dissolved in THF and loaded onto the top of a silica column (4 cm × 20 cm). The dark red product was eluted with MeOH, and solvent was removed with a rotary evaporator. The dried residue was triturated with H_2O and dried under vacuum to yield 0.049 g (0.061 mmol, 34.5%) of the pure product. The Et_4N^+ salt (**4TEA**) was obtained in an analogous manner starting from **1TEA**. Crystals of X-ray quality were obtained by cooling a saturated MeOH solution of **4TEA** at −5 °C for 2 weeks. IR (THF) ν(CO): 2046 (m); 1990 (s); 1975 (m); 1936 (w), cm^{-1}; ^1H NMR (DMSO): 4.28 (d, J = 12.7, 2H); 6.65 (d, J = 8.8 Hz, 2H); 7.40 (d, J = 8.8 Hz, 2H); 7.47 (m, 3H); 7.55 (m, 6H); 7.63 (m, 6H) ppm; Electronic absorption spectrum (H_2O): λ_{max} (ε, M^{-1} cm^{-1}) 489 (1260), 330 (9330), 303 (14210), 229 (15130), HRMS (ESI) m/z calcd for $C_{31}H_{23}Fe_2NO_8PS_3^{1-}$ Theoretical Mass: 775.9022 g/mol; Found Mass: 775.8988 g/mol.

Synthesis of Na(μ-$SCH_2N(C_6H_4SO_3)CH_2S$-)[$Fe(CO)_2PMe_3$], (5Na). To a slurry of **1Na**,(0.250 g, 0.44 mmol) in THF (20 mL) was added PMe_3, (0.5 mL, 4.2 mmol). The solution was then heated to 60 °C, and the solution was monitored by IR spectroscopy. After 4−6 h no ν(CO) bands were visible above 2000 cm^{-1}, and the reaction was stopped. The resulting dark red solution was concentrated to ~5−10 mL, and ether (50 mL) was added resulting in a red-purple precipitate. The solid was filtered under N_2 and rinsed on the filter with ether (30 mL), toluene (30 mL), and hexanes (30 mL). After drying under vacuum for 24 h, 0.181 g (0.273 mmol, 61.6%) of **5Na** was obtained. The Et_4N^+ salt (**5TEA**) was prepared in an analogous manner starting from **1TEA**. Crystals of X-ray quality were obtained by slow diffusion of ether into a CH_2Cl_2 solution of **5TEA**. IR (THF) ν(CO): 1982 (w); 1948 (s); 1903 (m), cm^{-1}; ^1H NMR (DMSO): 1.47 (d, J_{HP} = 9.28, 18H); 4.17 (s, 4H); 6.69 (d, J = 8.3 Hz, 2H); 7.39 (d, J = 8.3 Hz, 2H) ppm; Electronic absorption spectrum (H_2O): λ_{max} (ε, M^{-1} cm^{-1}) 517 (370), 352 (1300),

dx.doi.org/10.1021/ic200272x |*Inorg. Chem.* 2011, 50, 5015–5026

274 (3040), 247 (3400), HRMS (ESI) m/z calcd for $C_{18}H_{26}Fe_2NO_8P_2S_3^{1-}$ Theoretical Mass: 637.9045 g/mol; Found Mass: 637.9071 g/mol.

RESULTS AND DISCUSSION

Synthesis of Na(μ-SCH$_2$N(p-C$_6$H$_4$SO$_3^-$)CH$_2$S)[Fe(CO)$_3$][Fe(CO)$_2$L], L = P(OMe)$_3$ (2Na); PTA (3Na); or PPh$_3$ (4Na) and Na(μ-SCH$_2$N(p-C$_6$H$_4$SO$_3^-$)CH$_2$S)[Fe(CO)$_2$PMe$_3$]$_2$ (5Na). The condensation reaction between formaldehyde, an amine, and (μ-SH)$_2$[Fe(CO)$_3$]$_2$ to give (μ-SCH$_2$N(R)CH$_2$S)[Fe(CO)$_3$]$_2$ as reported by Rauchfuss and co-workers has become a widely used procedure for the incorporation of useful R groups into the dithiolate linker of diiron complexes as parent models of the [Fe—Fe]-Hydrogenase enzyme active site.[21] We have recently demonstrated that sulfanilic acid can be used in this method to introduce an aryl sulfonate group into the dithiolate linker of the model complexes to give the anionic (μ-SCH$_2$N(p-C$_6$H$_4$SO$_3^-$)CH$_2$S)[Fe(CO)$_3$]$_2$.[12] This compound acts as precursor to a series of water-soluble phosphine-substituted complexes through the synthetic routes shown in Scheme 1.

Treatment of **1Na** with 1 equiv of Me$_3$NO followed by either P(OMe)$_3$ or PPh$_3$ yielded the monosubstituted complexes **2Na** and **4Na**, respectively. The PTA derivative, **3Na**, was synthesized by heating a solution of **1Na** and multiple equivalents of the PTA ligand overnight. All of the monosubstituted complexes are obtained as air-stable red solids in moderate yield and can be isolated as the Na^+ salt as depicted in Scheme 1 or as the Et_4N^+ salt by direct synthesis from **1TEA** or by counterion exchange using Et_4NCl. ^{1}H NMR analysis of the complexes shows two signals for the methylene protons in the dithiolate linker of the monophosphine complexes, resulting from the loss of symmetry between the two irons upon substitution of a single CO. Table 1 lists the IR stretching frequencies in THF for the complexes shown in Scheme 1. As expected, ν(CO) stretching frequencies for the monosubstituted complexes are lower than those of **1Na**, consistent with the increased donation into the Fe atoms by the phosphine ligands versus CO; the increased electron density on Fe based on these ν(CO) values is in the order **3Na** > **4Na** > **2Na**.

The reaction of **1Na** with excess PMe$_3$ at 60 °C in THF gives the disubstituted complex **5Na** in ~60% yield. IR analysis of the product shows significantly lower ν(CO) stretching frequencies for **5Na** as compared to the monosubstituted complexes, consistent with the higher degree of substitution. ^{1}H NMR data find a single signal for the four methylene protons in the SRS linker at room temperature indicating that one phosphine has substituted onto each iron. Additionally, this single signal indicates that the sulfanilate moiety is flipping rapidly between both sides as is seen in the case of the (μ-pdt) analogue.[22] Unlike the stable monosubstituted complexes, **5Na** is air sensitive and degrades rapidly in solutions exposed to air. As a solid, **5Na** is air tolerant for short amounts of time; however, prolonged exposure also leads to decomposition.

Water Solubility of 2Na—5Na. The sulfonate group endows a degree of water solubility on (μ-SCH$_2$N(C$_6$H$_4$SO$_3^-$)CH$_2$-S-)[Fe(CO)$_2$L]$_2$ (L = CO or PR$_3$) that varies depending on the ligands. In the case of the parent hexacarbonyl complex, **1Na**, the maximum obtainable concentration was ~1.1 mM at 22 °C. Upon substitution, the solubilities vary depending on the nature

Table 1. IR Stretching Frequencies in the ν(CO) Region in THF for Complexes 1Na—5Na

complex	ν(CO) cm^{-1}
1Na[a]	2074 (w); 2035 (s); 1996 (m)
2Na	2048 (m); 1992 (s); 1971 (m); 1942 (w)
3Na	2042 (m); 1986 (s); 1967 (sh); 1930 (w)
4Na.	2046 (m); 1990 (s); 1975 (m); 1936 (w)
5Na	1982 (w); 1948 (s); 1903 (m)

[a] From ref 12; (s) strong; (m) medium; (w) weak; (sh) shoulder.

Table 2. Crystallographic Experimental Data for the Complexes

	1Na·THF	2TEA	3TEA	4TEA	5TEA
formula	$C_{18}H_{18}Fe_2NNaO_{11}S_3$	$C_{24}H_{37}Fe_2N_2O_{11}PS_3$	$C_{27}H_{40}Fe_2N_5O_8PS_3$	$C_{39}H_{43}Fe_2N_2O_8PS_3$	$C_{27}H_{46}Fe_2N_2O_8P_2S_3$
formula weight	655.20	768.41	801.49	906.60	796.48
temperature (K)	110(2)	110(2)	110(2)	110(2)	110(2)
wavelength (Å)	1.54178	0.71073	1.54178	1.54178	0.71073
Z	2	4	4	2	4
$D_{calc'd}$ (Mg/cm^3)	1.753	0.671	1.527	1.455	1.440
μ (mm^{-1})	12.436	0.509	9.241	7.838	1.092
crystal system	triclinic	orthorhombic	monoclinic	triclinic	monoclinic
space group	$P\bar{1}$	$Pca21$	$P2/n$	$P\bar{1}$	$P21/c$
unit cell					
a (Å)	6.4151(9)	14.046(14)	14.968(2)	10.1101(18)	10.311(2)
b (Å)	12.6371(9)	33.262(15)	7.6777(11)	11.2927(19)	34.159(7)
c (Å)	15.6834(16)	16.28(3)	30.718(4)	18.607(3)	10.437(2)
α	96.703(2)	90.00	90.00	102.336(6)	90
β	95.498(9)	90.00	99.042(7)	93.946(6)	91.713(2)
γ	98.239(10)	90.00	90.00	90.895(6)	90
volume (Å^3)	1241.5(2)	7606(18)	3486.3(9)	2069.4(6)	3674.4(12)
goodness-of-fit	1.045	0.962	1.030	1.029	1.065
R$_1$[a], wR$_2$[b](%) [$I > 2\sigma(I)$]	0.0840, 0.2325	0.0738, 0.1362	0.0806, 0.1543	0.0521, 0.0982	0.0428, 0.1036
R$_1$[a], wR$_2$[b](%) all data	0.1020, 0.2550	0.1649, 0.1692	0.1598, 0.1828	0.0937, 0.1080	0.0560, 0.1094

[a] $R_1 = \Sigma||F_o| - |F_c||/\Sigma|F_o|$. [b] $wR_2 = [\Sigma w(F_o^2 - F_c^2)^2/\Sigma w(F_o^2)^2]^{1/2}$.

dx.doi.org/10.1021/ic200272x |Inorg. Chem. 2011, 50, 5015–5026

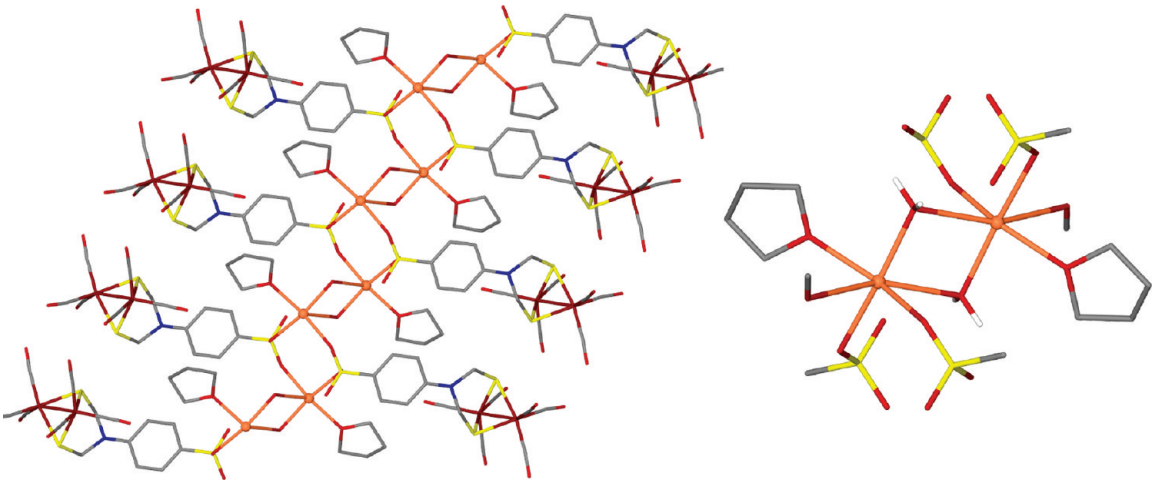

Figure 2. (Left) Extended structure of **1Na** as a stick model showing the sodium ion-controlled array in the solid state. Protons have been omitted for clarity and sodium ions are represented as balls. (Right) Close up view of the Na^+ ions showing the coordination environment around them. All protons except the water protons have been removed for clarity.

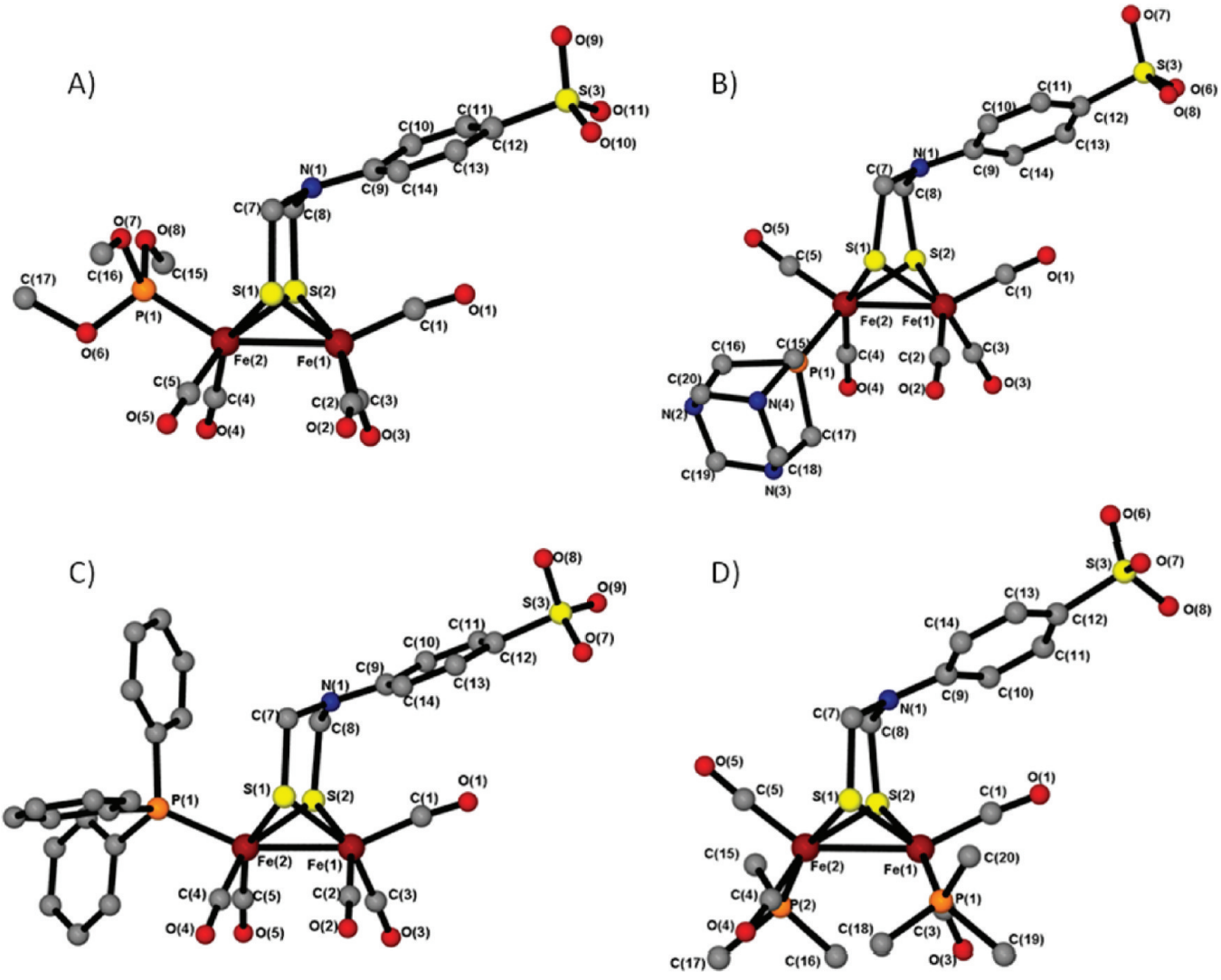

Figure 3. Solid states structures of (A) **2TEA**, (B) **3TEA**, (C) **4TEA**, and (D) **5TEA** as ball and stick models. Protons and the Et_4N^+ counterions have been omitted for clarity.

dx.doi.org/10.1021/ic200272x |*Inorg. Chem.* 2011, 50, 5015–5026

Table 3. Comparison of Selected Metric Data for 1Na, 1TEA,[12] and 1[23]

	1[23]	1TEA[12]	1Na
Fe−Fe	2.510(1)	2.498(1)	2.512(6)
Fe−C_{avg}	1.800	1.797	1.786
C−$O_{avg.}$	1.136	1.140	1.155
Fe(1)−S(1)	2.254(1)	2.251(1)	2.259(8)
Fe(1)−S(2)	2.249(1)	2.269(1)	2.282(7)
Fe(2)−S(1)	2.254(1)	2.257(1)	2.280(8)
Fe(2)−S(2)	2.249(1)	2.278(1)	2.275(8)
S(1)−C(7)	1.823(4)	1.860(5)	1.86(3)
S(2)−C(8)	1.818(4)	1.861(5)	1.79(3)
Fe(1)−S(1)−Fe(2)	67.67(4)	66.97(4)	66.8(2)
Fe(1)−S(2)−Fe(2)	67.85(4)	67.02(4)	67.3(2)
Fe(2)−Fe(1)−C(1)	148.3	147.4(1)	155.7(9)
Fe(1)−Fe(2)−C(6)	148.3	155.8(2)	148.1(1)
C(1)−Fe(1)−Fe(2)−C(6)	0	7.9(5)	25.7(1)

of the ligands. Both complexes **2Na** and **5Na** show slightly higher maximum concentrations, about 1.4−1.9 mM at 22 °C, than complex **1Na**. For complex **4Na**, the hydrophobic PPh_3 ligand dramatically reduces solubility and lowers the maximum concentration to <0.1 mM, making it the least water-soluble of the complexes. Conversely when the more hydrophilic PTA ligand is used the maximum concentration is greatly increased, with **3Na** dissolution of up to ∼3 mM in pure water. The significantly greater water solubility of the **3Na** complex makes it one of the most water-soluble diiron complexes reported to date. The CN^--containing complexes are expected to be even more water-soluble based on the original account by Pickett and coworkers;[6] however, no quantitative data on their solubilities was reported. It should be noted that the solubilities for all of the complexes were measured in pure water; the addition of small amounts of salt (NaCl, KCl, or Et_4NCl) results in partial precipitation of the complexes from solution.

Table 2 lists the crystal data for the five structures. While the structure of **1TEA** was recently reported, that of the sodium salt, **1Na**, was not.[12] Upon cooling a THF solution of **1Na** at 5 °C overnight in the presence of a small amount of water, large X-ray quality crystals grew. While similar to the Et_4N^+ structure, there are key differences between the two salts. The extended packing diagram of **1Na**, Figure 3, shows that two Na^+ ions interact with adjacent sulfonate groups and bridge between pairs of the diiron moieties. In addition to a THF solvent molecule that also binds to the Na^+, two water molecules connect each Na^+ to the Na^+ of an adjacent dimer to create a two-dimensional array of the diiron molecules in the solid state. Though not within bonding distance to the Na^+, an apical carbonyl O atom from an adjacent array at 2.933 Å blocks the sixth coordination site on the Na^+ leaving it with a pseudosquare pyramidal geometry. A long-range ion-dipole interaction between the Na^+ and the carbonyl oxygen could be the explanation for the increased C1−Fe1−Fe2-C6 torsion angle of **1Na**.

X-ray Diffraction Studies of 1Na and 2TEA−5TEA. Table 3 lists selected metric parameters of (μ-pdt)$[Fe(CO)_3]_2$ (**1**), **1TEA**, and **1Na**. In **1**[23] the $Fe(CO)_3$ units are eclipsed, and there is only a slight increase in the C1−Fe1−Fe2−C6 torsion angle between the apical carbonyl units for **1TEA**. However, when the Et_4N^+ counterion is exchanged for Na^+, this torsion angle increases by ∼18° (25° > **1**). In the [Fe−Fe]-H_2ase enzyme active site, a number of dipole−dipole and hydrogen bonding interactions are purported to stabilize the unique geometry and semibridging carbonyl.[1] The possibility that an ion dipole interaction in the model complexes could be used to enforce structural changes is thus intriguing.[24] Nevertheless, UV spectroscopic studies showed no discernible difference between **1TEA** and **1Na** in the solvents used in this study indicating that these interactions in **1Na** exist only in the confines of the solid state.

Table 4. Selected Metric Data for 2TEA−5TEA

	2TEA	3TEA	4TEA	5TEA
Fe−Fe	2.504(3)	2.532(2)	2.506(1)	2.600(1)
Fe−C_{avg}	1.836	1.759	1.768	1.763
C−$O_{avg.}$	1.106	1.169	1.143	1.154
Fe(1)−S(1)	2.572(3)	2.260(2)	2.274(1)	2.250(1)
Fe(1)−S(2)	2.571(2)	2.281(3)	2.269(1)	2.269(1)
Fe(2)−S(1)	2.186(3)	2.255(3)	2.271(1)	2.252(1)
Fe(2)−S(2)	2.170(2)	2.256(2)	2.281(1)	2.257(1)
S(1)−C(7)	1.984(7)	1.985(8)	1.852(5)	1.857(3)
S(2)−C(8)	1.984(8)	1.982(8)	1.854(5)	1.852(3)
Fe(1)−S(1)−Fe(2)	67.3(1)	68.23(8)	66.92(4)	70.57(3)
Fe(1)−S(2)−Fe(2)	68.3(1)	67.86(7)	66.83(4)	70.35(3)
Fe(2)−Fe(1)−C(1)	154.1(3)	152.6(3)	156.1(2)	152.6(1)
Fe(1)−Fe(2)−L_{apical}	149.0(1)	148.9(3)	156.19(5)	142.7(1)
C(1)−Fe(1)−Fe(2)−L_{apical}	5.0(7)	10.5(8)	9.8(5)	11.3(3)

Despite repeated attempts, crystals of X-ray quality were not obtained for the Na^+ salts of the substituted complexes; however, the respective Et_4N^+ salts (**2TEA−5TEA**) of the compounds readily crystallize from either slow diffusion of ether into a CH_2Cl_2 solution of the compounds or by cooling saturated MeOH solutions. The core structure of all four molecules contains the familiar 2Fe2S butterfly motif common to this class of compounds.[25] Additionally, both irons have a square based pyramidal geometry with the two sulfurs defining the shared edge between them. As is the normal case with the structures of most Fe^IFe^I model complexes the CO ligands are all terminal. The pyramidalization of the N in the dithiolate linker is very modest (ca. 0.1 to 0.2 Å above the C_3 plane around it) throughout the series of complexes and is similar to that observed for **1Na** and the corresponding aniline derivative which lacks the sulfonate group.[21]

The solid state structures of the monosubstituted complexes are consistent with the degrees of substitution indicated by the spectral data and are overall structurally similar to the analogous propanedithiolate complexes.[8,26] For **2TEA−4TEA** the phosphine ligands are situated on the iron distal to the aryl sulfonate group, likely to minimize steric repulsions between the ligand and the aryl group of the dithiolate. While the weaker donor ligands, $P(OMe)_3$ and PPh_3, adopt an apical position within their respective $FeS_2(CO)_2L$ square pyramids, the PTA ligand assumes a basal orientation consistent with its stronger donor ability and small size. The Fe−Fe bond distances for **2TEA−4TEA** remain similar throughout the series, Table 4, with only an ∼0.03 Å change from the weaker donor-containing complexes

dx.doi.org/10.1021/ic200272x |*Inorg. Chem.* 2011, 50, 5015–5026

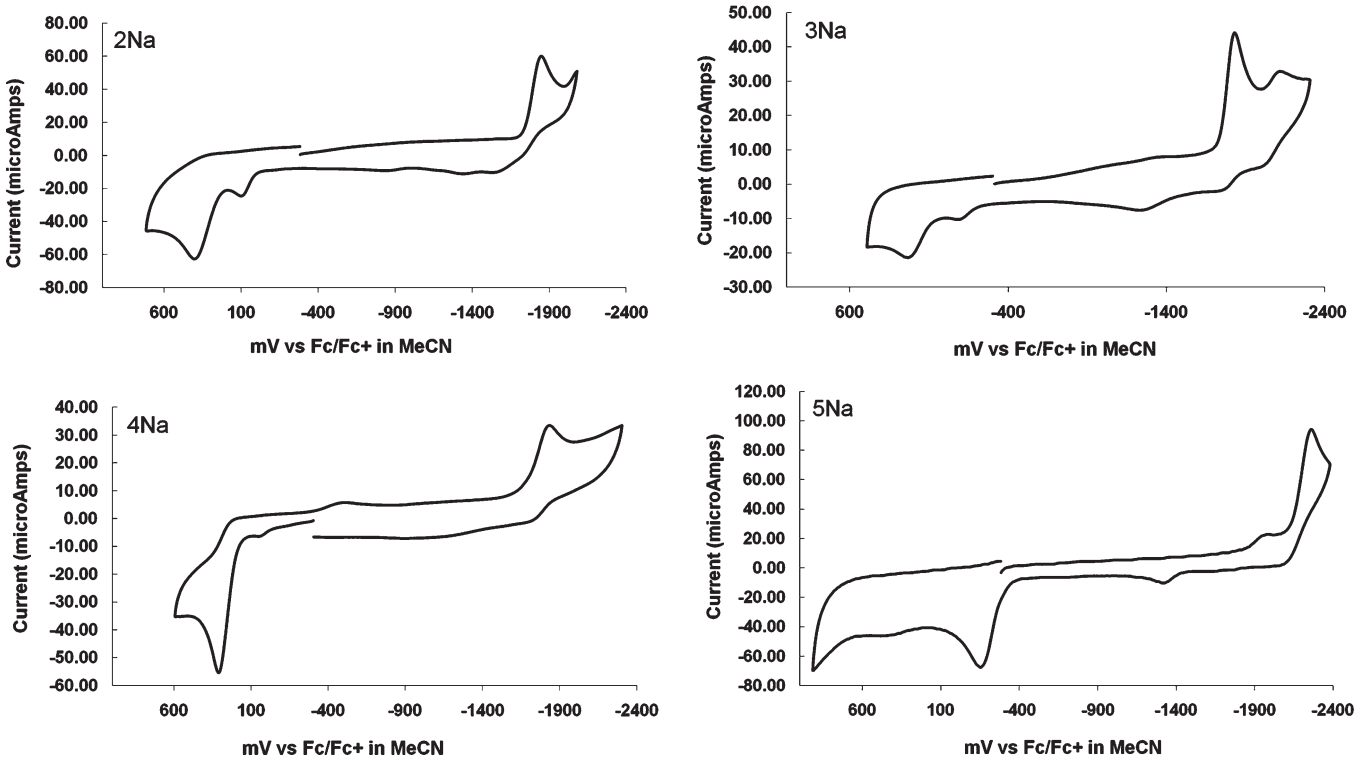

Figure 4. Cyclic voltammograms of complexes **2Na**, **3Na**, **4Na**, and **5Na** in MeCN with 0.1 M Bu_4NBF_4 at a scan rate of 200 mV/s. Concentration of all samples is 2 mM.

2TEA and **4TEA** to complex **3TEA**; they fall within the typical range for Fe−Fe bond distances found in the diiron model complexes, 2.49−2.56.[27] The similarities to previously reported systems means that the sulfonate group, while altering the solubilities, is far enough removed from the diiron unit to have influence on significant changes in the core structure and reactivity of the complexes.

The structure of **5TEA** shows similarities to both the monosubstituted complexes and its (μ-pdt) analogue. Both of the PMe_3 ligands adopt basal positions in the $FeS_2(CO)_2L$ square pyramids and are transoid to each other in the diiron structure. The core geometry and twisting between the two iron units, defined by the C1−Fe1−Fe2−C6 torsion angle, is only slightly larger than in the monosubstituted species. However, the Fe−Fe bond length of 2.600(1) Å in **5TEA** is significantly longer than most model complexes and is instead closer to the values reported for the enzyme active site (~2.6).[28] This value is also one of the largest reported for a Fe^IFe^I species, even among other disubstituted complexes.[27]

Interaction with β-Cyclodextrin. In addition to providing water solubility, the aryl sulfonate group also promotes interaction between the model complexes and β-cyclodextrin (β-CyD). Our recent description of the **1Na·2β-CyD** solid state structure, Figure 1A, showed that the aryl sulfonate group of the complex penetrates the cavity, putting the aromatic ring inside of the cyclodextrin with the sulfonate group protruding through the primary hydroxyl rim of the cyclodextrin.[12] Interestingly, the crystal structure also showed that a second cyclodextrin could interact with the $Fe(CO)_3$ unit opposite the aryl sulfonate, though no evidence of such an interaction was observed in solution. The ν(CO) IR spectra of the all-CO parent sulfonate, **1 Na** in water shows a band pattern and positions typical of all (μ-SRS)$[Fe(CO)_3]_2$ complexes, 2077 m, 2041 s, 2002 s. On addition of 10 equiv of β-cyclodextrin, minor band shifts are observed: 2079, 2042 (s), 2008 (s), see Supporting Information, Figure S8.

Nuclear Magnetic Resonance (NMR) studies on the interaction of cyclodextrins with guest molecules find greater changes for the inward directed C3 and C5 protons on the cyclodextrin as compared to the other protons.[29] While the direction and magnitude of this change is dependent on the nature of the group inside the cyclodextrin cavity, aromatic groups typically result in an increased shielding of the C3 and C5 protons and thus an upfield shift. An upfield shift is also generally observed for the protons on the aromatic guest molecule. This was the case observed for **1Na** and these same resonances were used in studying the substituted derivatives. The NMR studies, conducted in D_2O and focused on the dependence of both the phosphine substituted complexes and the cyclodextrin ^1H chemical shifts on the ratio of the two components, indicate that all of the substituted complexes can interact with cyclodextrin (see Supporting Information); however, the specific nature of this interaction varies throughout the series.

For complex **2Na**, as the ratio of β-CyD to **2Na** is increased, there is an upfield shift of the aromatic proton resonances of the aryl sulfonate group from 7.68 and 6.92 ppm for pure **2Na** to 7.51 and 6.79 ppm at a CyD/**2Na** ratio of 9:1. Additionally, moderate shifts in the C3 and C5 proton resonances of the cyclodextrin are observed when the ratio is reversed to 1:9 of CyD/**2Na**. Shifts of this magnitude are consistent with an interaction between the iron complex and the cyclodextrin and are similar to those observed for **1Na**.[12] Additionally because the changes in chemical shift for the cyclodextrin occur primarily for the C3 and C5 protons, which are oriented toward the interior cavity of the cyclodextrin, the behavior is consistent with inclusion in the cavity of the cyclodextrin. Similar effects are observed for **3Na** as

dx.doi.org/10.1021/ic200272x |*Inorg. Chem.* 2011, 50, 5015–5026

well with shifts occurring primarily for the C3 and C5 protons of the cyclodextrin and the aryl protons on the aromatic ring of the model complex. Interestingly, for **3Na** changes are also observed for the methylene protons of the PTA ligand with the resonance at 4.05 ppm shifting downfield to 4.09 ppm. While not large, this shift could still indicate some interaction between the PTA ligand and the cyclodextrin, possibly through hydrogen bonding between the hydroxyl groups of the cyclodextrin and the amines. However, as only one set of signals is observed for both the host and guest components, the strength of the binding or rate of dissociation and association does not appear to have been significantly altered, relative to **1Na**, by any such interaction.

Complex **5Na** causes significantly different changes in the chemical shifts of the cyclodextrin proton resonances. As the ratio of **5Na**:CyD is increased the C5 proton resonance behaves in a manner similar to the other complexes, shifting upfield from 3.75 to 3.64 ppm. However, the C3 proton resonance now shifts downfield from 3.89 to 3.94 ppm. Additionally, there is an upfield shift for the C4 proton resonance from 3.51 to 3.48 ppm. Despite the difference in the resonances for the cyclodextrin, the aryl protons on the diiron complex show a similar upfield shift upon increasing the ratio of cyclodextrin to **5Na** as observed for the other complexes. All of these changes indicate that **5Na** interacts with cyclodextrins in solution; however, the discrepancies between the NMR data for **5Na** and the other sulfonated complexes implies that it interacts in a different manner. One possibility is that the aryl sulfonate is entering the cyclodextrin cavity from the primary hydroxyl side, preventing full penetration and positioning the sulfonate group closer to the C3 proton.

Table 5. Electrochemical Data for 2Na−5Na in MeCN[a]

complex	Ep_c (V)	Ep_a (V)
1Na[12]	−1.61	0.59
2Na	−1.85	0.40
3Na	−1.81	0.22
4Na.	−1.85	0.31
5Na	−2.24	−0.19

[a] Ar deaerated CH_3CN solution (0.1 M $^nBu_4NBF_4$). All experiments were recorded using a glassy carbon working electrode (A = 0.071 cm^2) referenced to Cp_2Fe/Cp_2Fe^+ as an internal standard and a Pt counter electrode at a scan rate of 200 mV/s.

Electrochemical Studies of 2Na−5Na in MeCN. In MeCN, the complexes show similar electrochemical events as have been reported for the analogous diiron systems with different dithiolates,[5] with both an irreversible Fe^IFe^I/Fe^IFe^0 reduction and irreversible Fe^IFe^I/Fe^IFe^{II} oxidation, Figure 4 and Table 5. For complexes **2Na** and **3Na**, a second oxidative event appears at about 100 mV. This event is not present when the reductive scan is stopped prior to the Fe^IFe^I/Fe^IFe^0 reduction and is thus attributed to a degradation product of the first reduction. While all of the oxidative events follow the expected trend based on the donor abilities of the ligands as established from ν(CO) infrared studies, the reductive events do not, and instead the monosubstituted complexes are all reduced at ∼−1.8 V. More interesting is the fact that the stronger donor containing complex, **3Na**, is reduced at slightly more positive potentials than either **2Na** or **4Na**. The differences are more pronounced in their electrochemical response to HOAc, added as a proton source for electrocatalytic reduction of H^+ to H_2.

For complex **2Na** dissolved in MeCN, upon addition of HOAc an increase in the current response of the reductive event

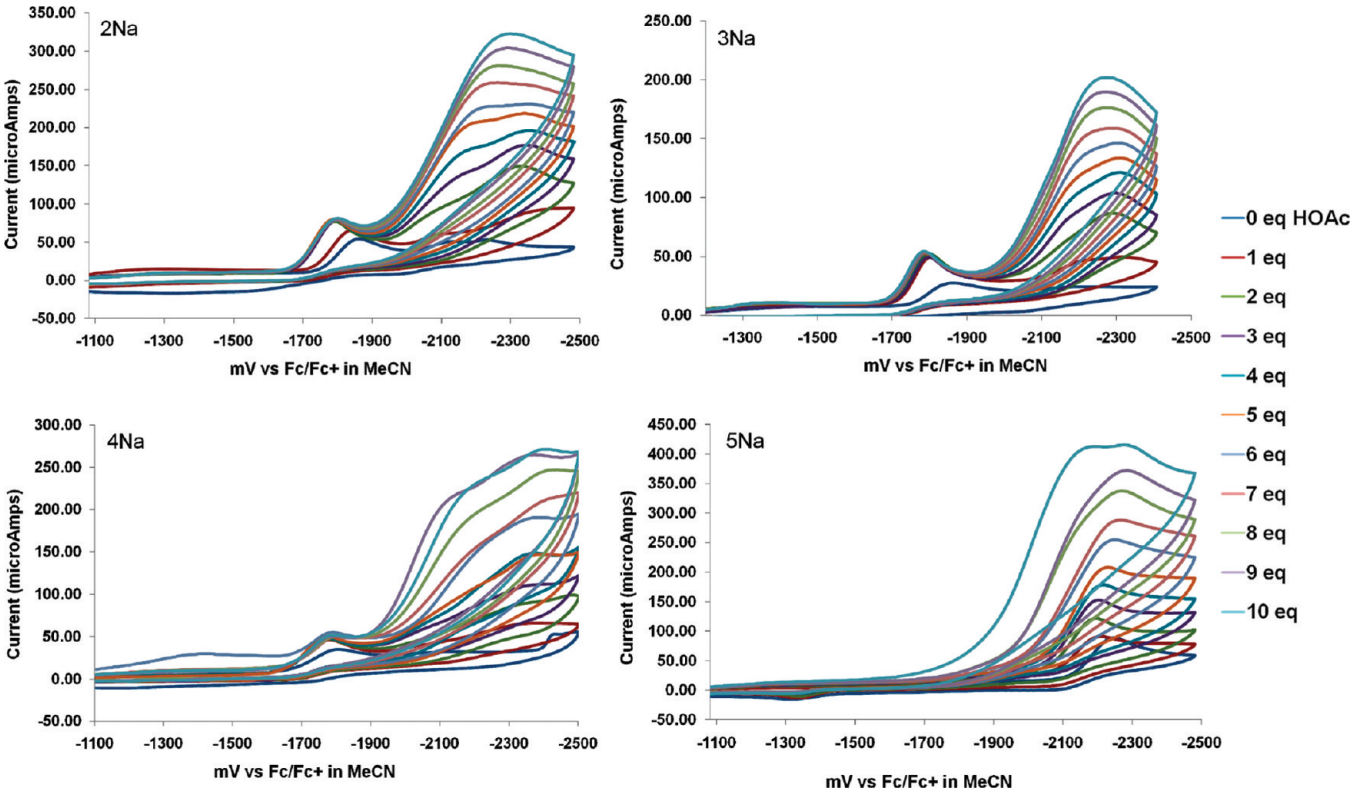

Figure 5. Cyclic voltammograms of complexes **2Na**, **3Na**, **4Na**, and **5Na** in MeCN with 0.1 M Bu_4NBF_4 at a scan rate of 200 mV/s showing the effect of added HOAc. Concentration of all samples is 2 mM.

dx.doi.org/10.1021/ic200272x |*Inorg. Chem.* 2011, 50, 5015–5026

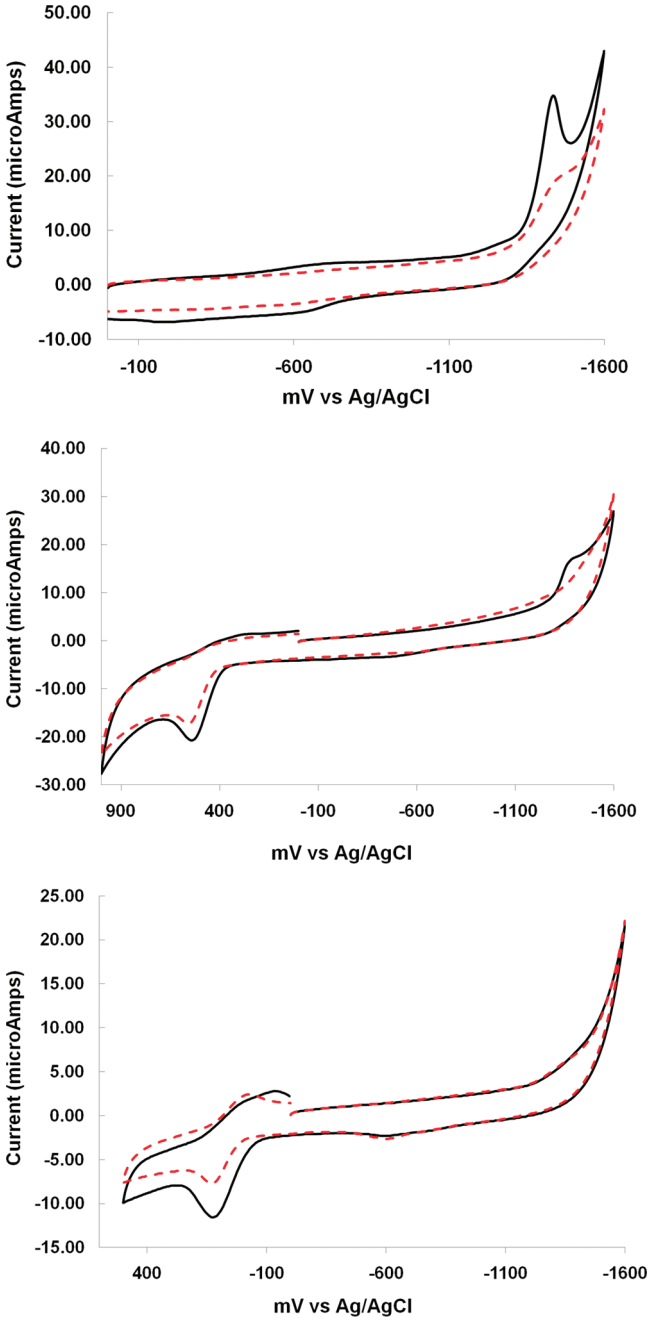

Figure 6. Cyclic voltammograms of complexes (Top) **2Na**; (Middle) **3Na**; (Bottom) **5Na** in 0.01 M aqueous NaCl in the absence (black line) and presence (red line) of 1 mM β-cyclodextrin. Scans were run at 200 mV/s with sample concentration of 0.1 mM.

around −2.10 V is observed and distinguishable from the event attributed to reduction of HOAc on glassy carbon, Figure 5. The fact that this response occurs at potentials past the initial reduction of **2Na** is consistent with trends reported for the less electron rich model complexes.[17,30−35] Similarly, complexes **3Na** and **4Na** exhibit an increase in the current well beyond their first reductive events, −2.24 and −2.15 V, respectively. While both **2Na** and **3Na** show an anodic shift for this event at higher concentrations of HOAc, the increase observed in **4Na** shifts to more positive potentials with incremental addition of the acid similar to the behavior observed in **5Na**. Unlike the other

Table 6. Electrochemical Data for 2Na−5Na in H_2O[a]

Complex	Ep_c (V) [With CyD]	Ep_a (V) [With CyD]
1Na[12]	−1.22 [−1.31]	0.78 [0.82]
2Na	−1.45 [−1.47]	0.71 [0.68]
3Na	−1.39 [*b*]	0.54 [0.53]
5Na	*b*	0.13 [0.13]

[a] Ar deaerated H_2O solution (0.01 M NaCl). All experiments were recorded using a glassy carbon working electrode (A = 0.071 cm^2) referenced to Ag/AgCl (sat'd KCl) and a Pt counter electrode at a scan rate of 200 mV/s. [b] Reduction is beyond the solvent window.

substituted complexes **5Na** shows a response to HOAc at the first reduction potential, that with subsequent additions of acid splits into two distinguishable redox events at −2.15 and −2.26 mV. Figure 7 shows plots of the change in current versus the equivalents of acetic acid. The slopes for best fit lines in all of the complexes indicate a similar response for the reduction of H^+ from HOAc.[7]

Electrochemical Studies of 2Na−5Na in H_2O. The increased water solubility of the complexes permits electrochemical examination in aqueous solutions. Similar to MeCN solutions, most of the compounds in H_2O show both an irreversible oxidation and reduction, Figure 6 and Table 6. Similar to what was observed in MeCN the reductive events of **2Na** and **4Na** are in a similar range, −1.39 to −1.45 V, and are not entirely consistent with expected changes resulting from the donor abilities of the ligands. For complex **5Na** the reductive event seen in MeCN solution is not observed and is likely beyond the solvent window. While the data for comparison of the aqueous electrochemistry to other diiron model complexes is still strongly limited by the scarcity of water-soluble systems, comparison of **3Na** to the similar ligand substituted DAPTA complex by Sun and co-workers shows that the two compounds have similar reductive events at −1.45 and −1.5 respectively.[9] Complexes **2Na** and **5Na** adsorb onto the surface of the glassy carbon electrode, resulting in changes in the observed potentials for the redox events, and require continual cleaning of the electrode to reproduce the events of the initial scan. At no point do the sulfonate species react with water; they are surprisingly stable, showing no change in the electrochemical response after being left in deaerated solution for several hours.

In the presence of β-cyclodextrin, all of the complexes show noted decreases in the current intensity associated with both the reductive and the oxidative events. This is commonly seen in other electrochemical studies of inclusion complexes and is attributed to the slower diffusion of the host−guest complex relative to the free guest.[36] The reductive events also show minor differences in the potentials with the initial reduction of **3Na** shifting more cathodic by greater than 100 mV. (This is best seen by DPV displays.) By comparison, the oxidative events only shift at most between 30 and 40 mV, also more cathodic. A change in the reduction event of ~80 mV was noted for **1Na** in the presence of cyclodextrin.[12] The hydrophobic nature of the cyclodextrin cavity likely plays a large role in this difference with the neutral oxidized species being less disfavored than the dianionic reduced species and thus shifted to more accessible potentials while the reduction is shifted to more negative potentials.[15]

The electrochemical response to HOAc was also studied for the water-soluble complexes in aqueous solutions. Because the first reduction is beyond the solvent window and complex **5Na** does not react with HOAc, the changes in its voltammograms with added

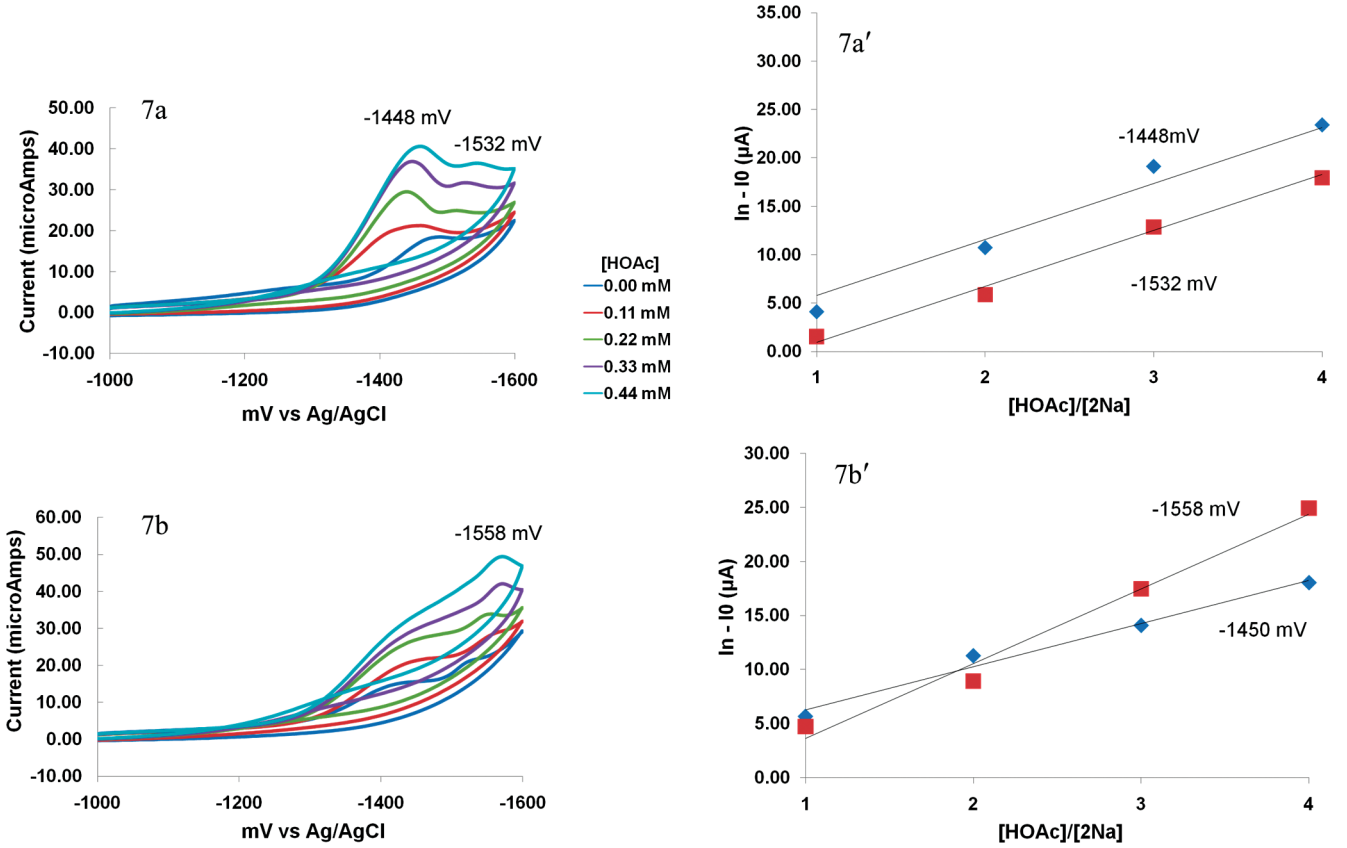

Figure 7. Aqueous cyclic voltammograms of complexes **2Na** in the absence (top, 7a) and presence (bottom, 7b) of 10 equiv of β-CyD, showing the response to incremental addition of HOAc. Scans were run at 200 mV/s with samples concentration of 0.1 mM. Next to each set of voltammograms, 7a′ and 7b′, are plots of the change in current versus equivalents of HOAc for points near the two observed events −1450 (diamonds) and −1550 mV (squares). Note that whereas the responses of the events in 7a/7a′ parallel each other, for 7b/7b′ the more positive event at −1450 mV is less responsive in the presence of β-CyD.

HOAc are indistinguishable from voltammograms of pure HOAc increments itself. However, for complexes **2Na** and **3Na** there are notable changes in the current intensities for the reductive events similar to that observed for the parent complex **1Na**. Upon addition of HOAc to a solution of **2Na**, there is an increase in current for the $Fe^{I}Fe^{I}/Fe^{I}Fe^{0}$ reduction at −1.45 mV, Figure 7. A second event about 100 mV more cathodic is also observed to increase with increasing $[H^{+}]$, and with a similar response slope, Figure 7a′. The presence of multiple events for proton reduction is not surprising as this is generally the case when proton reduction studies are carried out in MeCN. Evans and co-workers have proposed that these separate events, observed in MeCN for $(\mu\text{-pdt})[Fe(CO)_3]_2$, are due to conformational changes that occur upon reduction resulting in multiple conformers that reduce protons at different potentials.[37] Of further interest to this notion is that when this proton reduction assay is carried out in the presence of β-cyclodextrin, Figure 7b, the more anodic of the two responses is less affected by the β-CyD. That this change in the ratio of these responses could be resulting from limited mobility inside of the cyclodextrin cavity is an intriguing prospect that parallels the concept that the geometry of the enzyme active site can be held in place by the surrounding peptide architecture.

CONCLUSIONS

The facile incorporation of the sulfonate group into the dithiolate of the diiron hexacarbonyl and P-donor ligand substituted derivatives has resulted in greatly increased water solubility as compared to the widely studied propane-dithiolate analogues. The aryl sulfonate approach shows significant advantages over reported methods for developing water-soluble diiron complexes including (1) the facile synthesis of a variety of water-soluble, CO-substituted derivatives; (2) the stability of resulting complexes in oxygen free water for several hours; and (3) the promotion of the interaction between the diiron complex and β-cyclodextrin which greatly enhances the water solubility.

Despite the advantages, this series has other problems; the amphiphilic nature of the sulfonate complexes leads to adsorption of the compounds onto the glassy carbon electrode and fouling of the electrode surface results. This problem is slightly resolved by balancing out the complex using the more hydrophilic PTA ligand or encapsulation in the cyclodextrins; however, it is not completely eliminated. A more dynamic electrode surface, such as that obtained through use of a mercury drop electrode,[7] could lead to a better understanding of the electrochemistry of these water-soluble species. It is clear that mechanistic studies of electrocatalytic behavior are best performed in nonaqueous solvents which might in fact more accurately match the dielectric of the [FeFe]-H_2ase active site. In either case, once optimal biomimetics are designed, through correlation of synthetic advances, electrochemical, and mechanistic advances, the engineering of solid phase matrixes with H_2O delivery routes will be required for applications.

dx.doi.org/10.1021/ic200272x |*Inorg. Chem.* 2011, 50, 5015–5026

■ ASSOCIATED CONTENT

Supporting Information. Full structure files, cyclic voltammograms, and spectral data. This material is available free of charge via the Internet at http://pubs.acs.org.

■ AUTHOR INFORMATION

Corresponding Author
*E-mail: marcetta@mail.chem.tamu.edu.

■ ACKNOWLEDGMENT

We gratefully acknowledge financial support from the National Science Foundation (Grant CHE-0910679) and the Robert A. Welch Foundation (Grant A-0924). We appreciate the help of Jason Denny in the final preparation of the structure tables and figures.

■ REFERENCES

(1) Nicolet, Y.; Lemon, B. J.; Fontecilla-Camps, J. C.; Peters, J. W. *Trends Biochem. Sci.* **2000**, *25*, 138.
(2) Hambourger, M.; Gervaldo, M.; Svedruzic, D.; King, P. W.; Gust, D.; Ghirardi, M.; Moore, A. L.; Moore, T. A. *J. Am. Chem. Soc.* **2008**, *130*, 2015.
(3) Esswein, A. J.; Nocera, D. G. *Chem. Rev.* **2007**, *107*, 4022.
(4) Tard, C.; Pickett, C. J. *Chem. Rev.* **2009**, *109*, 2245.
(5) Felton, G. A. N.; Mebi, C. A.; Petro, B. J.; Vannucci, A. K.; Evans, D. H.; Glass, R. S.; Lichtenberger, D. L. *J. Organomet. Chem.* **2009**, *694*, 2681.
(6) Le Cloirec, A.; Davies, S. C.; Evans, D. J.; Hughes, D. L.; Pickett, C. J.; Best, S. P.; Borg, S. *Chem. Commun.* **1999**, 2285.
(7) Felton, G. A. N.; Glass, R. S.; Lichtenberger, D. L.; Evans, D. H. *Inorg. Chem.* **2006**, *45*, 9181.
(8) Mejia-Rodriguez, R.; Chong, D.; Reibenspies, J. H.; Soriaga, M. P.; Darensbourg, M. Y. *J. Am. Chem. Soc.* **2004**, *126*, 12004.
(9) Na, Y.; Wang, M.; Jin, K.; Zhang, R.; Sun, L. *J. Organomet. Chem.* **2006**, *691*, 5045.
(10) Li, P.; Wang, M.; Chen, L.; Wang, N.; Zhang, T.; Sun, L. *CrystEngComm* **2008**, *10*, 267.
(11) Apfel, U.-P.; Halpin, Y.; Gottschaldt, M.; Goerls, H.; Vos, J. G.; Weigand, W. *Eur. J. Inorg. Chem.* **2008**, 5112.
(12) Singleton, M. L.; Reibenspies, J. H.; Darensbourg, M. Y. *J. Am. Chem. Soc.* **2010**, *132*, 8870.
(13) Breslow, R.; Dong, S. D. *Chem. Rev.* **1998**, *98*, 1997.
(14) Hapiot, F.; Tilloy, S.; Monflier, E. *Chem. Rev.* **2006**, *106*, 767.
(15) Johnson, M. D.; Bernard, J. G. *Chem. Commun.* **1996**, *2*, 185.
(16) Kano, K. *Colloid Polym. Sci.* **2008**, *286*, 79.
(17) Surawatanawong, P.; Tye, J. W.; Darensbourg, M. Y.; Hall, M. B. *Dalton Trans.* **2010**, *39*, 3093.
(18) Spek, A. L. *J. Appl. Crystallogr.* **2003**, *36*, 7–13.
(19) (a) *APEX2*; Bruker AXS Inc.: Madison, WI, 2007. (b) *GADDS*; Bruker AXS Inc.: Madison, WI, 2007. (c) *SAINT*; Bruker AXS Inc.: Madison, WI, 2007. (d) Sheldrick, G. M. *Acta Crystallogr.* **2008**, *A64*, 112.
(20) Barbour, L. J. *J. Supramol. Chem.* **2003**, *1*, 189.
(21) Li, H.; Rauchfuss, T. B. *J. Am. Chem. Soc.* **2002**, *124*, 726.
(22) Lyon, E. J.; Georgakaki, I. P.; Reibenspies, J. H.; Darensbourg, M. Y. *J. Am. Chem. Soc.* **2001**, *123*, 3268.
(23) Lyon, E. J.; Georgakaki, I. P.; Reibenspies, J. H.; Darensbourg, M. Y. *Angew. Chem.* **1999**, *38*, 3178.
(24) Liu, Y.-C.; Tu, L.-K.; Yen, T.-H.; Lee, G.-H.; Chiang, M.-H. *Dalton Trans.* **2011**, *40*, 2528.
(25) Wei, C. H.; Dahl, L. F. *Inorg. Chem.* **1965**, *4*, 1.
(26) Li, P.; Wang, M.; He, C.; Li, G.; Liu, X.; Chen, C.; Åkermark, B.; Sun, L. *Eur. J. Inorg. Chem.* **2005**, 2506.
(27) Singleton, M. L.; Jenkins, R. M.; Klemashevich, C. L.; Darensbourg, M. Y. *C. R. Chim.* **2008**, *11*, 861.
(28) Fontecilla-Camps, J. C.; Volbeda, A.; Cavazza, C.; Nicolet, Y. *Chem. Rev.* **2007**, *107*, 4273.
(29) Schneider, H.-J.; Hacket, F.; Ruediger, V.; Ikeda, H. *Chem. Rev.* **1998**, *98*, 1755.
(30) Capon, J.-F.; Ezzaher, S.; Gloaguen, F.; Pétillon, F. Y.; Schollhammer, P.; Talarmin, J.; Davin, T. J.; McGrady, J. E.; Muir, K. W. *New J. Chem.* **2007**, *31*, 2052.
(31) Gloaguen, F.; Morvan, D.; Capon, J.-F.; Schollhammer, P.; Talarmin, J. *J. Electroanal. Chem.* **2007**, *603*, 15.
(32) Capon, J.-F.; Ezzaher, S.; Gloaguen, F.; Pétillon, F. Y.; Schollhammer, P.; Talarmin, J. *Chem.—Eur. J.* **2008**, *14*, 1954.
(33) Capon, J.-F.; Gloaguen, F.; Pétillon, F. Y.; Schollhammer, P.; Talarmin, J. *Coord. Chem. Rev.* **2009**, *253*, 1476.
(34) Chong, D.; Georgakaki, I. P.; Mejia-Rodriguez, R.; Sanabria-Chinchilla, J.; Soriaga, M. P.; Darensbourg, M. Y. *Dalton Trans.* **2003**, 4158.
(35) Tye, J. W.; Lee, J.; Wang, H.-W.; Mejia-Rodriguez, R.; Reibenspies, J. H.; Hall, M. B.; Darensbourg, M. Y. *Inorg. Chem.* **2005**, *44*, 5550.
(36) Matsue, T.; Evans, D. H.; Osa, T.; Kobayashi, N. *J. Am. Chem. Soc.* **1985**, *107*, 3411.
(37) Felton, G. A. N.; Petro, B. J.; Glass, R. S.; Lichtenberger, D. L.; Evans, D. H. *J. Am. Chem. Soc.* **2009**, *131*, 11290.

■ NOTE ADDED AFTER ASAP PUBLICATION

This paper was published on the Web on April 27, 2011. The in-text citations of refs 23 and 28 have been corrected and the updated version was reposted on May 2, 2011.